Article

Customizable Fabrication Process for Flexible Carbon-Based Electrochemical Biosensors

Catalin Marculescu [1,*] ![ORCID], **Petruta Preda** [1,*], **Tiberiu Burinaru** [1,2], **Eugen Chiriac** [1,3], **Bianca Tincu** [1] ![ORCID], **Alina Matei** [1] ![ORCID], **Oana Brincoveanu** [1], **Cristina Pachiu** [1] **and Marioara Avram** [1] ![ORCID]

[1] National Institute for Research and Development in Microtechnologies—IMT Bucharest, 126A Erou Iancu Nicolae, 077190 Bucharest, Romania
[2] Faculty of Veterinary Medicine, University of Agronomic Sciences and Veterinary Medicine, Splaiul Independenței 105, 050097 Bucharest, Romania
[3] Faculty of Applied Chemistry and Material Science, University "Politehnica" of Bucharest, 313 Splaiul Independent, Ei, 060042 Bucharest, Romania
* Correspondence: catalin.marculescu@imt.ro (C.M.); petruta.preda@imt.ro (P.P.)

Abstract: In recent research, 3D printing has become a powerful technique and has been applied in the last few years to carbon-based materials. A new generation of 3D-printed electrodes, more affordable and easier to obtain due to rapid prototyping techniques, has emerged. We propose a customizable fabrication process for flexible (and rigid) carbon-based biosensors, from biosensor design to printable conductive inks. The electrochemical biosensors were obtained on a 50 μm Kapton® (polyimide) substrate and transferred to a 500 μm PDMS substrate, using a 3D-extrusion-based printing method. The main features of our fabrication process consist of short-time customization implementation, fast small-to-medium batch production, ease of electrochemical spectroscopy measurements, and very good resolution for an extrusion-based printing method (100 μm). The sensors were designed for future integration into a smart wound dressing for wound monitoring and other biomedical applications. We increased their sensibility with electro-deposited gold nanoparticles. To assess the biosensors' functionality, we performed surface functionalization with specific anti-N-protein antibodies for SARS-CoV 2 virus, with promising preliminary results.

Keywords: carbon-based electrochemical biosensors; 3D printing; flexible sensors; electrochemical impedance spectroscopy

1. Introduction

Also known as additive manufacturing (AM) or rapid prototyping, 3D printing technologies can be used to make parts from 3D computer-aided design (CAD) models. This is a powerful technique that has been employed in research activities as well as in industrial production in many fields such as medicine, aerospace, catalysis, etc. Because this process has been applied in the last few years to carbon-based materials, it still faces many challenges in obtaining directly printed carbon, such as optimizing the printed material and the matrix in which it is incorporated [1]. Due to their excellent properties, some of the most extensively used materials for 3D printing are carbonaceous materials such as carbon nanotubes [2], carbon fibers [3,4], carbon black [5,6], graphene, and graphene oxide [7,8].

Recent advances in this field have enabled the use of 3D printing for fabricating electrochemical sensors or biosensors that can be used in different areas. Conventionally manufactured electrodes such as glassy carbon, screen-printed, and composite carbon electrodes could be replaced by a new generation of 3D-printed electrodes that are more affordable and easier to obtain due to rapid prototyping techniques [9–15]. In recent years, the applications that have raised the most interest are wearable and portable flexible sensors, soft robotics, and implantable biomedical devices that can be miniaturized and tailored to suit the end users [16,17]. There have been several reports regarding wearable and flexible

invasive or non-invasive electrochemical biosensors for the real-time monitoring of glucose, lactate, dopamine, cortisol, or antigens of interest [18–22]. Carbon-based nanomaterials have been used to develop conductive platforms for flexible electrochemical biosensor fabrication. There are several advantages to using this type of material for healthcare monitoring and clinical analysis: excellent biocompatibility, low costs, ease of fabrication and personalization using rapid prototyping, light weight, high stretchability, and high performance due to the intrinsic properties of the two-dimensional nanomaterials.

In this study, we propose a customizable fabrication process for flexible (and rigid) 3D-printed carbon-based biosensors for electrochemical impedance spectroscopy, from biosensor design to printable conductive inks. Some of these features are reported in the literature, but, to our knowledge, no study comprises all of them.

Zhao et al. developed an invasive electrochemical sensor using a flexible electrode based on a three-dimensional (3D) monolithic nanoporous gold scaffold (NPG) supported by graphene paper (GP) enhanced with platinum cobalt (PtCo) alloy nanoparticles for the detection of glucose. Their sensor showed a broad linear range from 35 μM to 30 mM, a limit of detection (LOD) of 5μM, and a sensitivity of 7.84 μA cm^{-2} mM^{-1} [23]. Lee et al. also reported a graphene gold-doped biosensor fabricated using chemical vapor deposition (CVD) that measures glucose levels, thus creating a wearable sweat-focused patch for diabetes monitoring and therapy [24].

Britton et al. developed a flexible strain-responsive sensor fabricated from a biocompatible electronic ink via an additive-manufacturing process. They used an environmentally sustainable copolymer-x-pentadecalactone-co-e-decalactone (PDL) that incorporates silver nanowires (AgNWs). The device demonstrated a low electrical resistance (320 $\pm$ 9 O/sq) and a high electrical capacitance (2.06 $\pm$ 0.06 mF/cm^2). They also demonstrated biocompatibility through in vitro testing by promoting neural adhesion and prevention of astrocyte activation. The biosensors were tested by monitoring approximately one million biologically relevant strain cycles [25].

Tang et al. developed micro-supercapacitors (MSCs) using a new type of hybrid-dimensional Fe$_2$O$_3$/graphene/Ag ink, performing direct-ink writing-based three-dimensional (3D) printing. The device had a maximum area capacitance of 412.3 mF cm^{-2} at 2 mA cm^{-2}, a correspondingly high energy density of 65.4 μWh cm^{-2}, and 89% capacitance retention for over 5000 charge and discharge cycles. The 3D-printed MSC exhibited reliable flexibility with remarkable retention of 90.2% of its original capacitance after 500 bending cycles [26].

Silva Neto et al. developed a 3D-printed bath injection method for the analysis of BIA cells integrated with eight sensing electrodes in a single step. The electrodes were modified with graphene oxide. The device was printed within 3.4 h using a multi-material printer equipped with insulating, flexible, and conductive filaments at a cost of ca. USD 1.2 per unit. The device was tested using adrenaline (ADR) as the target analyte. The fully 3D-printed system provided suitable analytical performance in terms of repeatability and reproducibility (RSD $\leq$ 6%), linear concentration range (5 to 40 μmol L^{-1}; R2 = 0.99), the limit of detection (0.61 μmol L^{-1}), and high analytical frequency (494 $\pm$ 13 h^{-1}). The device was also tested on urine samples spiked with adrenaline solutions, with recovery values ranging from 87% to 118% [27].

The fabrication process is rarely a standalone process and often requires additional steps in product development (Scheme 1). In our case, the customizable fabrication process can include the customization of the sensors' design and the materials used: the conductive inks and substrates. The main features of our fabrication process consist of its short-time customization implementation, fast small-to-medium batch production (10–20 pieces batch can be produced in a couple of hours, while the same batch requires several days to weeks using the photolithography fabrication process, depending on its complexity and the equipment load), ease of electrochemical spectroscopy measurements, and very good resolution for an extrusion-based printing method (100 μm).
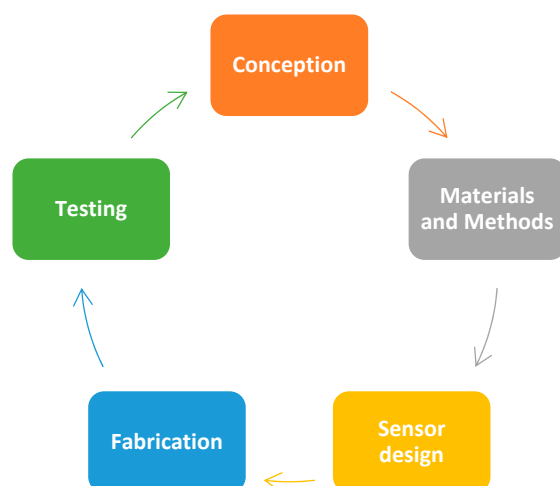
Scheme 1. The fabrication process integration in the sensors' development stages.

When developing complex instruments (e.g., lab-on-chip, point-of-care devices, etc.) aimed to increase the population welfare or simply to reduce the costs of the testing and/or monitoring of chronic diseases, you need a certain degree of flexibility and even freedom in your material choice and the structural design. This flexibility and freedom can be achieved using an extrusion-based bioprinter. The versatility of our bioprinter Allevi 1 allows for the use of a large range of inks, from medium–low to high viscosities (up to 400 Pa.s), thus allowing for the customization of the conductive inks.

The fabrication process presented in this work was optimized using several designs, but only two types of commercial conductive inks with known characteristics were used for printing to have better control over the process.

The sensors were designed for future integration into a smart wound dressing for wound monitoring and other biomedical applications. To assess the biosensors' functionality, we performed surface functionalization with specific anti-N-protein antibodies for SARS-CoV 2 virus, with promising preliminary results, which provide quantitative information on the changes in the electrochemical signal. A similar methodology was used by Tabrizi and Acedo in 2022, for the determination of SARS-CoV-2-RBD using a carbon nanofiber–gold nanocomposite-modified screen-printed electrode [4].

2. Materials and Methods

2.1. Materials and Reagents

Potassium hexacyanoferrate (III) K_3 [Fe(CN)$_6$] ($\geq$99.0 %, Sigma-Aldrich, Saint Louis, MO, USA), chloroauric acid (HAuCl$_4 \cdot$3H$_2$O, $\geq$99.9 %, Sigma-Aldrich, Saint Louis, MO, USA), H$_2$SO$_4$ (95.0–98.0%, Sigma-Aldrich, Saint Louis, MO, USA), KCl ($\geq$99%, Sigma-Aldrich, USA) and HCl (37%, Sigma-Aldrich, Saint Louis, MO, USA), 11-mercaptondecanoic acid (MUDA, 98%, Sigma-Aldrich, Saint Louis, MO, USA), 1-(3-dimethylaminopropyl)-3-ethylcarbodiimide hydrochloride, (EDC, $\geq$98%, Alfa Aesar, Tewksbury, MA, USA), bovine serum albumin (BSA, Sigma-Aldrich, Auckland, New Zealand), N-hydroxysuccinimide (NHS, 98%, Sigma-Aldrich, Tokyo, Japan) and 4-morpholineethanesulphonic acid (MES, $\geq$99.5 %, Sigma-Aldrich, Saint Louis, MO, USA), SARS-CoV-2 nucleocapsid protein mouse monoclonal antibodies (HyTest, Turku, Finland), SARS-CoV-2 nucleocapsid protein, recombinant (HyTest, Turku, Finland).

For the fabrication of the working electrodes (WEs) and the counter electrodes (CEs), a carbon-based ink with high viscosity (250–300 Pa.s, CH-8, Jelcon corp., Tokyo, Japan) was used, covered partially for insulation with epoxy resin (Deve Prodexim, Oradea, Romania). For the fabrication of reference electrodes (REs), a silver-based ink with medium viscosity (1–2 Pa.s, DM-SIP-3105S, Dycotec Materials Ltd., Calne, UK) was used. We opted for these inks as both are designed for flexible printed circuits. Additionally, a potentiostat, Autolab PGSTAT204 with a FRA32M electrochemical impedance spectroscopy (EIS) module

(METROHM AUTOLAB AG. Utrecht, The Netherlands), and the Nova 2.1.3 software were used for all electrochemical studies.

2.2. Electrochemical Sensor Fabrication Process

The fabrication process for the bioprinted electrochemical sensors (Figure 1) involved the following steps:

1. Substrate preparation—A 50 μm thick adhesive sheet of polyimide (Kapton®) was cut into the required dimensions (25 × 10 mm) and fixed onto a rigid support substrate with the same dimensions. The rigid substrate can be any type of material that can withstand up to 200 °C. In our case, we used a piece of a silicon wafer cut to the desired dimensions.
2. Electrodes printing—After the substrate was cleaned with isopropanol and dried with air jets, the prepared substrate was fixed onto the plate of the bioprinter Allevi 1. Two dispensers were loaded with the necessary pastes: the CH8 carbon paste and the Dycotec silver paste. The pastes were extruded onto the Kapton substrate starting with the Ag and finishing with the CH8. The printing parameters used for the extrusion process were the following: extrusion pressure (p) was 3 bar for the Ag and 5 bar for the CH8, and the printing head speed (V) was 20 mm/s for the Ag, and 10 to 20 mm/s for the CH8, respectively, depending on the electrode design. The printing parameters were optimized after a series of tests based on the printing ink viscosities.
3. Thermal treatment—Following the conductive ink deposition, thermal treatment was carried out for drying the extruded inks. Both inks have similar requirements; therefore, only one step of thermal treatment was performed: 30 min at 140 °C on a hotplate.
4. Transfer from the rigid substrate to the flexible substrate—The last step in this workflow was the transfer of the printed Kapton from the rigid support substrate to a flexible support substrate. The Kapton adhesive sheet was carefully peeled from the rigid substrate and placed on the flexible substrate. In this case, we used a 500 μm PDMS substrate that fits the same dimensions and that can be used in a SATA 2 connector.
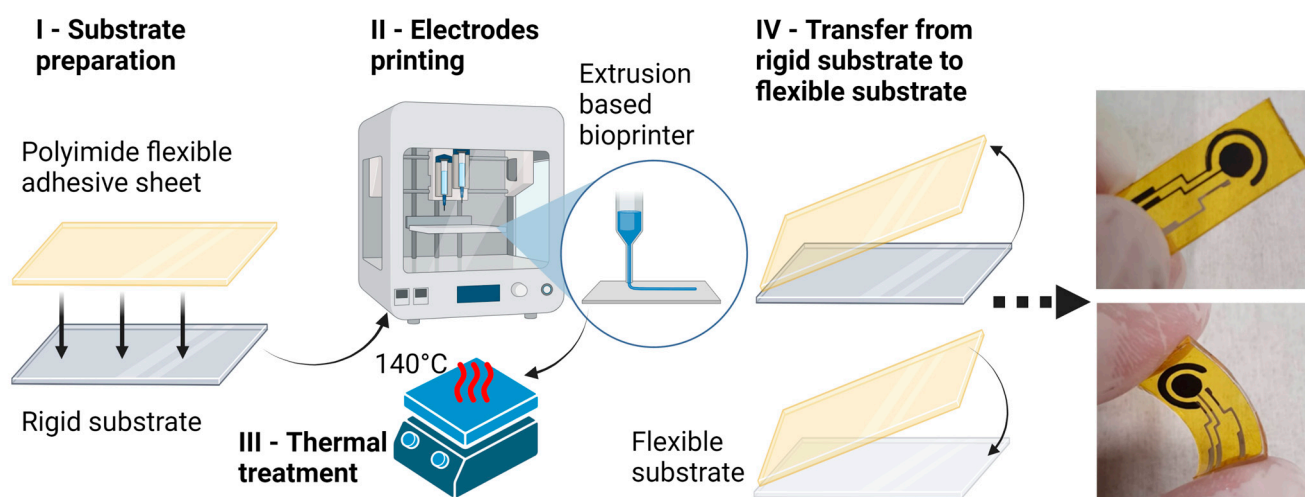

Figure 1. Fabrication process workflow.

Electrical insulation, completely covering the conductive routes and delimiting the WE, CE, and RE electrodes, was performed with low-viscosity bicomponent laminating epoxy resin.

2.3. Reference Electrode Preparation

The silver reference electrode was subjected to electrochemical chlorination using an Autolab PGSTAT204 potentiostat. The process consisted of using the potentiometric stripping analysis (PSA) option with a constant current of 10 mA for 0.5 s and placing a drop of 0.1 M HCl solution onto the electrodes. When the process concluded, the formation of silver chloride (AgCl) was confirmed with visual observation (wetted area darkening).

2.4. Carbon-Based Electrode Preparation

The printed electrodes were subjected to washing and cleaning processes using an Autolab PGSTAT204 potentiostat. The process consisted of three steps: (i) three cycles of cyclic voltammetry (CV) with a potential window from -0.1 to 0.6 V at a scanning rate of 50 mV/s and placing a drop of phosphate-buffered saline (PBS) solution containing 1 mM $[Fe(CN)_6]^{3-/4-}$ and 0.1 M KCl on the electrodes, to assess the oxidative processes; (ii) three cycles in CV with a potential window from -0.6 to 0.1 V at a scanning rate of 50 mV/s, to assess the reductive processes; and lastly (iii) washing with H_2O.

2.5. Surface Modification of the Working Electrode

The working electrodes were used in the decoration process of gold nanoparticles (AuNPs) using an Autolab PGSTAT204 potentiostat. The process consisted of 1 to 10 cycles of cyclic voltammetry (CV) with a potential window from 0.05 to 0.85 V at a scanning rate of 10 to 100 mV/s and placing a drop of 0.5 M H_2SO_4 in 2 mM $HAuCl_4$ solution on the electrodes. Variations in the number of cycles and the scanning rate were set to identify the optimal setup for the current application on our in-house fabricated sensors.

The decoration of the working electrode with AuNPs served for the specific functionalization of the sensor. The conjugation of AuNPs with specific antibodies was adapted from Higa et al. [28]. The immobilization of SARS-CoV-2 antibodies to AuNPs was made by incubating 20 μL of linker solution of 11-mercaptondecanoic acid (MUDA, 2 mM, in ethanol) for 2 h. The modification of the surface of AuNPs with MUDA was achieved through the thiol group (-SH) from the structure, via Au–S bond formation. After, the substrates were washed thoroughly with PBS and incubated for 1 h using a mixture of EDC (75 mM) and NHS (15 mM) obtained in MES buffer (25 mM) to activate the carboxyl group from MUDA for protein binding. Subsequently, after washing with PBS (pH 7.4), the 20 μL of SARS-CoV-2 nucleocapsid antibodies (20 μg/mL) were added to the working electrode and incubated for 1 h. Then, a 1% solution of BSA was used for 1 h to block unreacted ester–NHS groups and to minimize nonspecific adsorption. The functionalized bioprinted sensors were stored overnight at 2–8 °C, until functionality testing. To demonstrate the functionality of the sensor, they were incubated for 1 h with 20 μL N-protein solution (SARS-CoV-2 nucleocapsid protein) at 1 fM concentration. After washing with PBS, electrochemical measurements were performed. All the stages of functionalization were performed at room temperature (25 °C) in a humid atmosphere.

2.6. Morphological Characterization

The morphological characterization of the bioprinted working electrodes was performed to analyze the surface of the working electrode, as well as the size, distribution, and shape of the nanoparticles attached to the surface of the electrode. This characterization was carried out via scanning electron microscopy (SEM) using Nova NanoSEM 630 (FEI Company, Hillsboro, OR, USA).

2.7. Spectrometric Characterization

The spectrometric characterization of the bioprinted working electrodes was carried out to assess the modification on the surface of the working electrodes with the AuNPs and N-protein. Raman spectra were obtained using a WiTec Raman spectrometer (Alpha-SNOM 300S, WiTec. GmbH, Kroppach, Germany) with a back-scattering collection. Its excitation radiation was set at 532 nm from an Nd-YAG laser with a power of 10 mW, with 600

grooves/mm grating and 20 s acquisition time. The spectra were obtained using the WiTec Project Five software and processed (peak identification) with the Origin 8.5 software.

2.8. Electrochemical Characterization

As part of the characterization of the bioprinted working electrodes, cyclic voltammetry and impedance spectroscopy (EIS) techniques were used to study the degree of the modification of the electrode surface. A CV study was performed using a PBS solution containing 1 mM $[Fe(CN)_6]^{3-/4-}$ and 0.1 M KCl, where a 15 μL drop from the solution was placed on the bioprinted electrodes, and a CV scan was then performed with a potential window from −0.4 to 0.4 V at a scan rate of 100 mV/s. For the EIS study, a drop of PBS solution containing 1 mM $[Fe(CN)_6]^{3-/4-}$ and 0.1 M KCl was placed and analyzed using a range of frequencies starting from 1 MHz to 0.1 Hz.

3. Results

3.1. Electrochemical Sensor Fabrication Process

Following the fabrication process (Figure 1) presented in the previous section, we built in-house flexible and rigid carbon-based electrochemical sensors. We chose and successfully adopted two designs (Figure 2) used in the industry (e.g., Zimmer and Peacock sensors, Royston, UK) to test the fabrication process. The sensors were designed using a CAD/CAM specialized software program (Autodesk® Fusion 360™, Autodesk, Inc., San Rafael, CA, United States) that provided the gcode file necessary for the bioprinter. The WE geometric areas were 12.6 mm^2 for the circular design (Figure 2a,b) and 3.5 mm^2 for the linear one (Figures 2c and 3). To ease the electrochemical spectroscopy measurements, we redesigned the connecting pads, along with the sensor's dimensions, to fit either 8 SATA 2 connector pins (Figure 2c) or 15 SATA 2 connector pins (Figure 3). The corresponding pins were accordingly connected as inputs for the Autolab PGSTAT204 potentiostat. We tested several various designs of the flexible in-house printed sensors to determine the optimal configuration.
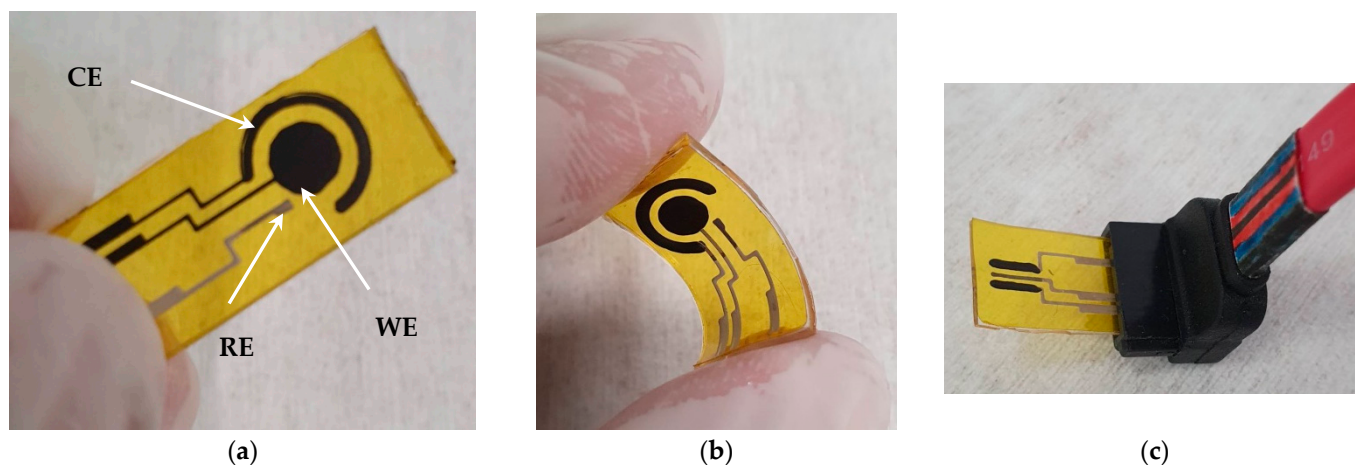

(a) (b) (c)

Figure 2. An electrochemical carbon-based sensor on a flexible substrate (25 × 10 mm) with 3 electrodes: (**a**) WE and CE were completely from carbon, and RE was Ag/AgCl; (**b**,**c**) all electrodes, electric routes, and pads were made from Ag, and in the interest area, WE and CE were covered with carbon paste.
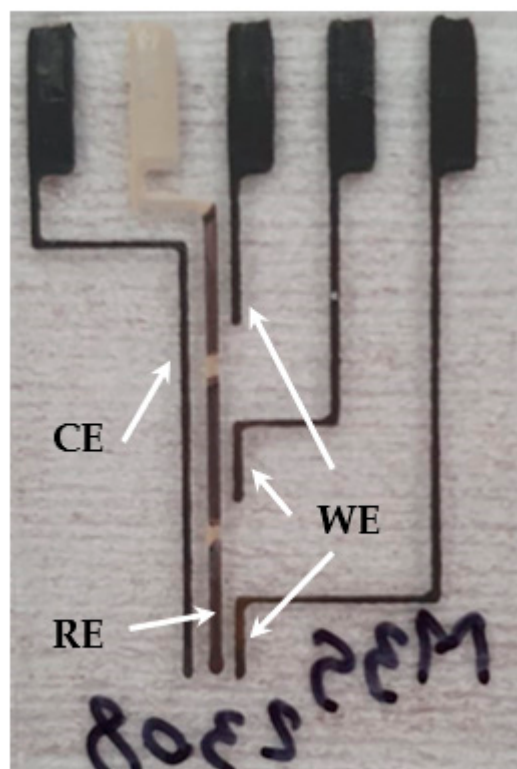
Figure 3. Electrochemical sensor array with 3 carbon-based sensors on a rigid substrate (30 × 20 mm), with 5 electrodes: WEx3 and CEx1 were completely carbon-based, and REx1 was made from Ag/AgCl.

The first variants were fully printed with the silver paste: The electrodes, electric routes, pads, and the interest areas of WE and CE were subsequently covered with carbon paste after the first thermal treatment to dry Ag deposition (Figure 2b,c). This was a laborious process, with high precision requirements to cover the existing routes and maintain the sensor integrity. It proved not to be the best approach, confirmed using the early CV measurements, which indicated additional peaks due to the silver–carbon interface (Figure A1). Therefore, to improve the printing stage and the quality of the sensors, we turned to a different approach. We printed with silver paste only the reference electrode, with its electric routes and pads. The rest of the electrodes (WE and CE) were fully printed with CH8, including the electric routes and pads (Figures 2a and 3). This proved to be a very good choice as CV and EIS measurements stabilized and improved considerably, along with lowering the complexity and duration of the fabrication process. We managed to print a batch of 20 sensors in less than 1 h, with a cost per unit of around USD 3. This sum is mainly from the equipment exploitation, the materials used are either very cheap (PDMS and Kapton) or used in very low quantities (the conductive inks).

3.2. Morphological Characterization

Using Nova NanoSEM 630, we were able to obtain the SEM micrographs of the AuNPs electro-deposited, to assess the influence of different parameters, such as the number of cycles or the scan rate value, on the AuNP formation (Table 1). The results highlight that the best results are given by the electro-deposition methods with at least 10 cycles and a scan rate lower than 50 mV/s. Similar results have been obtained by Drobysh et al. in 2022 [29]. Taking this under consideration, we chose two flexible sensors for the electrochemical characterization: S6/02.08 and S7/02.08.

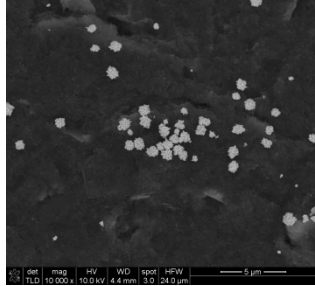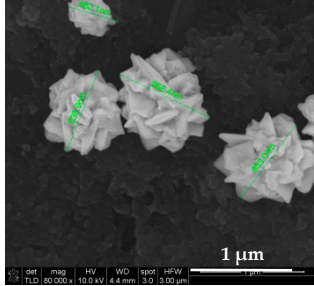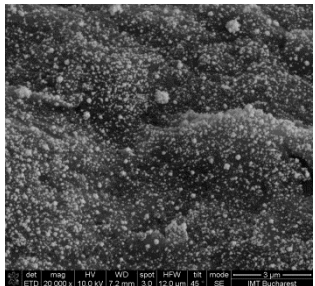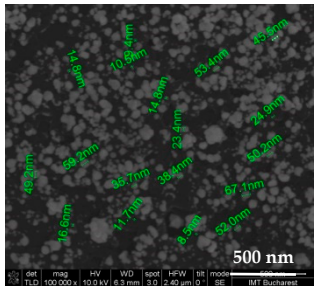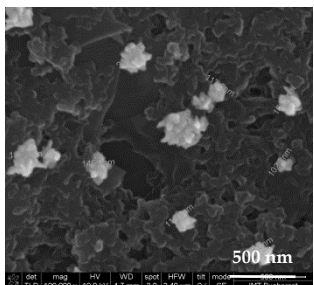**Table 1.** Influence of different parameters on the AuNP electro-deposition.
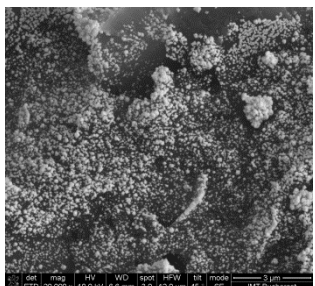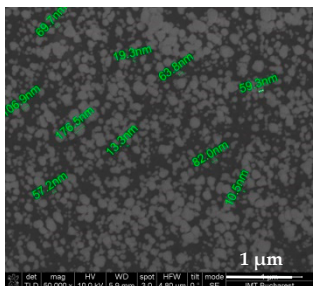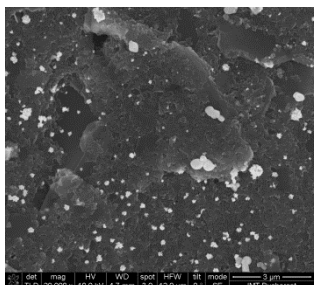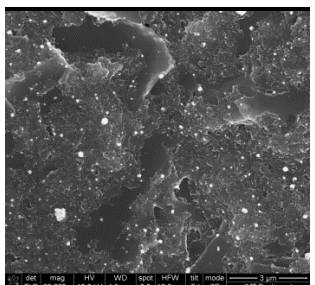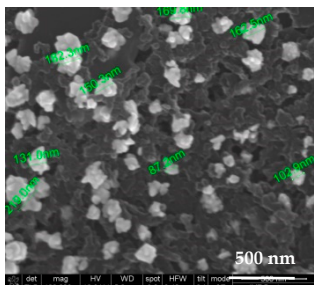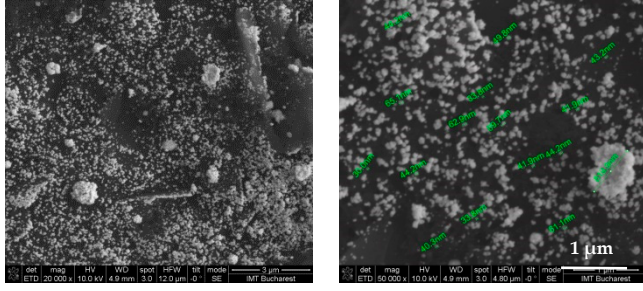
Sensor (Internal Denomination)	Scan Rate	No. of Cycles	Density	Size	SEM Micrographs	
S5/02.08	100 mV/s	10	Low	800 nm		
S6/02.08	50 mV/s	10	High	20–100 nm		
S7/02.08	10 mV/s	10	High	30–120 nm		
M3 S1/23.08	10 mV/s	1	Medium-Low	50–110 nm		
M3 S2/23.08	10 mV/s	5	Medium-Low	100–180 nm		

Table 1. *Cont.*

Sensor (Internal Denomination)	Scan Rate	No. of Cycles	Density	Size	SEM Micrographs	
M3 S3/23.08	10 mV/s	10	High	30–70 nm		

The size distribution of AuNPs was extracted from SEM micrographs by measuring 200 individual nanoparticles. The AuNPs' diameter sizes, determined based on SEM analysis, were found to range from 23 nm to 94 nm for S6/02.08 (Figure 4, left) and from 30 nm to 120 for S7/02.08 (Figure 4, right).
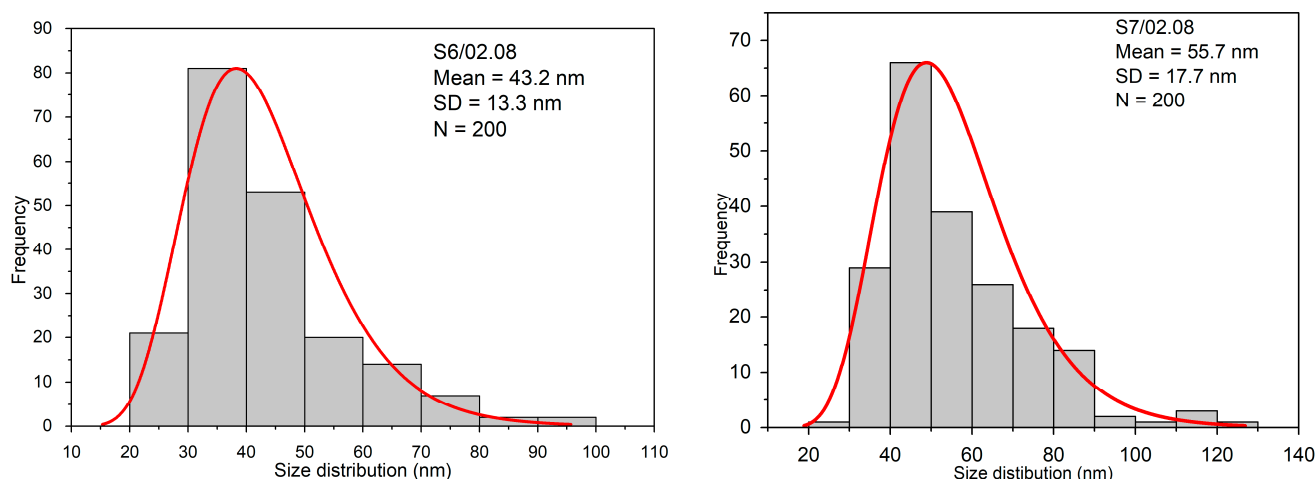

Figure 4. The size distribution of AuNPs for S6/02.08 (**left**) and S7/02.08 (**right**).

The histogram was best fitted with the Gauss function. The highest percentage of S6/02.08 NPs were found to be within the 30–50 nm diameter size range having a mean diameter of 43.2 ± 13.3 nm and S7/02.08 NPs were found to be within the 40–60 nm diameter size range having a mean diameter 55.7 ± 17.7 nm.

3.3. Spectrometric Characterization

The carbonic composition present on the working electrode, three prominent modes are highlighted: at ~1344 cm^{-1}, the noted D band, which is characteristic of carbonic defects, disordered sp3 bonded carbon typically observed in commercially available carbon paste; at ~1574 cm^{-1}, in the G band, E2g mode corresponds to the in-plane stretching of ordered sp2 bonded carbon and at ~2685 cm^{-1} is also representative of graphite; the secondary D mode was observed even without any disorder or defects [30].

Compared with the Raman spectrum of the carbonic working electrode (N-protein in our case, Figure 5 left; black spectrum), the adsorption of gold nanoparticles (Figure 5 left; red spectrum), did not result in the appearance of novel bands. Moreover, the two carbonic bands D and G where the intensity diminished illustrated a complete coverage of the active area with the AuNp film.
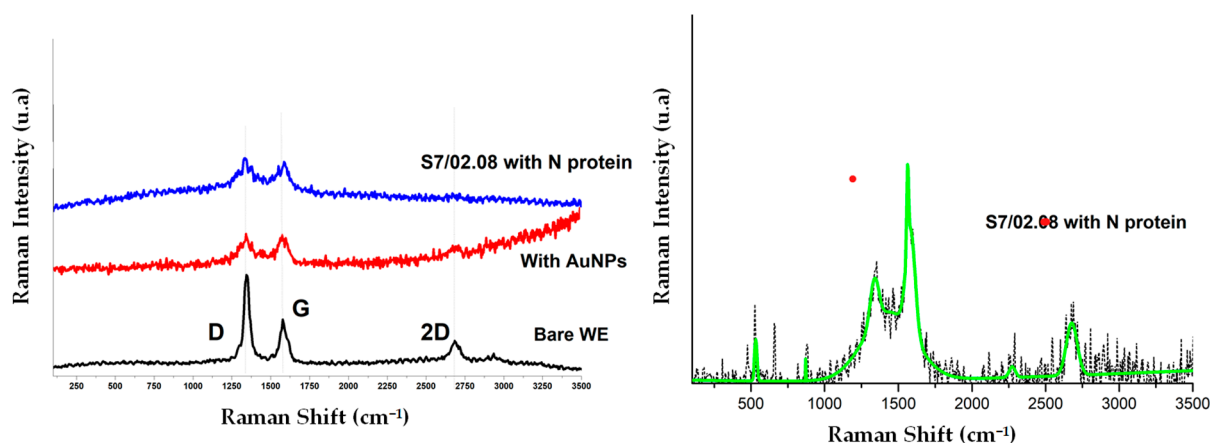
Figure 5. Raman spectra of WE: bare WE (black), with AuNPs (red) and with N-protein (**left**), with detail (blue) for S7/02.08 with N-protein (**right**).

The Raman intensities associated with protein subgroup vibrations (Figure 5 left, blue spectrum) are the representative Raman bands for organic bonds (C=O, C-N, and C-C in the region of 1033 cm^{-1} to 1200 cm^{-1}) and C–O bonds, as well as the modes of hydrogen substituents (e.g., C–H at 1444 cm^{-1}, N–H, or O–H at 823 cm^{-1}) [31]. The C–S and S–S vibrations of Met and Cys and the S–H vibrations of cysteine were localized around 1300 cm^{-1} and 1600 cm^{-1} covered in this case by the specific carbon modes (Figure 5 right; detail for blue Raman spectrum).

3.4. Electrochemical Characterization

The CV study was performed to demonstrate the functionality of the sensor. The results can be found in the Appendix A (Figures A1 and A2).

On the other hand, the EIS study revealed the influence of each surface modification on the sensor resistivity (Figure 6 for S6/02.08 and Figure 7 for S7/02.08) and phase shift (Figure 8 for S6/02.08 and Figure 9 for S7/02.08). Measurements were performed after each important step in the surface modification: AuNP decoration, antibody immobilization, and N-protein binding. For both cases, the measurements for MUDA functionalization and antibody immobilization were performed in one single step. To keep the electrochemically active surface area constant and to avoid cross-contamination, all the surface modifications and measurements were subsequently performed on the same day.

After decorating the electrodes with AuNPs, the charge transfer resistance (Rct) decreased from 7090 Ω to 372 Ω, indicating the increase in the transport rate of redox species at the electrode surface (Figures 6 and 7). Additionally, the admittance of the constant phase element (CPE) increased from 987 nS·s^N (N = 0.949) to 8.82 μS·s^N (N = 0.917) after decorating the electrode with AuNPs, due to the increase in the sensitive area of the working electrode. After 11-mercaptoundecanoic acid (MUDA) immobilization, Rct increased to 30,100 Ω, and after the incubation of SARS-CoV-2 virus N-protein, it increased to 39,200 Ω due to the reactive species transfer blocking to the electrode surface (Figure 7). The phase difference between electric current and potential decreased from 60° to 28° after AuNP decoration, indicating the increase in electrode surface conductivity, and then increased to 70° after protein N incubation, indicating a decrease in surface conductivity (Figure 8). The admittance of the CPE element slightly decreased, remaining at the same order of magnitude of 2 μS·s^N after N-protein incubation (Figure 7). EIS and CV characterizations indicated changes in the transfer rate of reactive species after each step of the functionalization of the sensing surface.
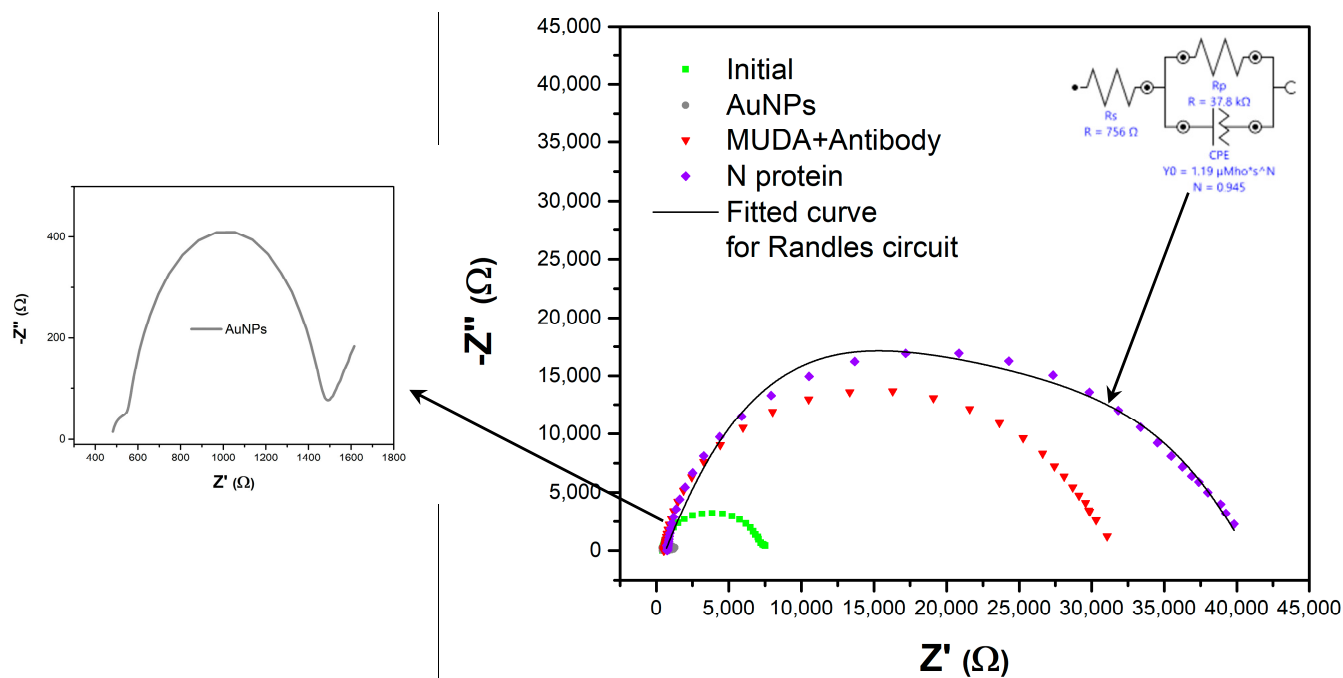
Figure 6. Nyquist diagram for the S6/02.08 sensor (WE area = 12.6 mm^2) with measurements after AuNP decoration, MUDA functionalization + antibody immobilization (one step), and N-protein binding.

Figure 7. Nyquist diagram for the S7/02.08 sensor (WE area = 12.6 mm^2) with measurements after AuNP decoration, MUDA functionalization + antibody immobilization (one step), and N-protein binding.
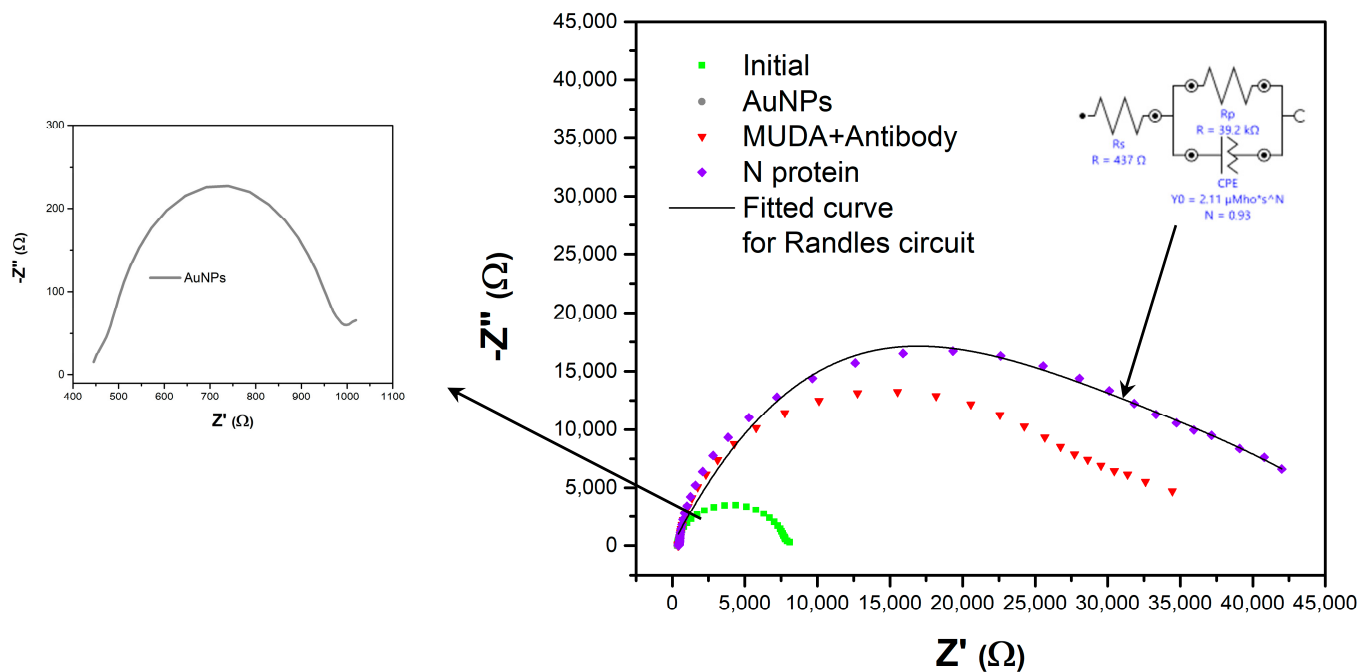
Figure 8. Bode diagram for the S6/02.08 sensor (WE area = 12.6 mm^2) with measurements after AuNP decoration, MUDA functionalization + antibody immobilization (one step), and N-protein binding.

Figure 9. Bode diagram for the S7/02.08 sensor (WE area = 12.6 mm^2) with measurements after AuNP decoration, MUDA functionalization + antibody immobilization (one step), and N-protein binding.
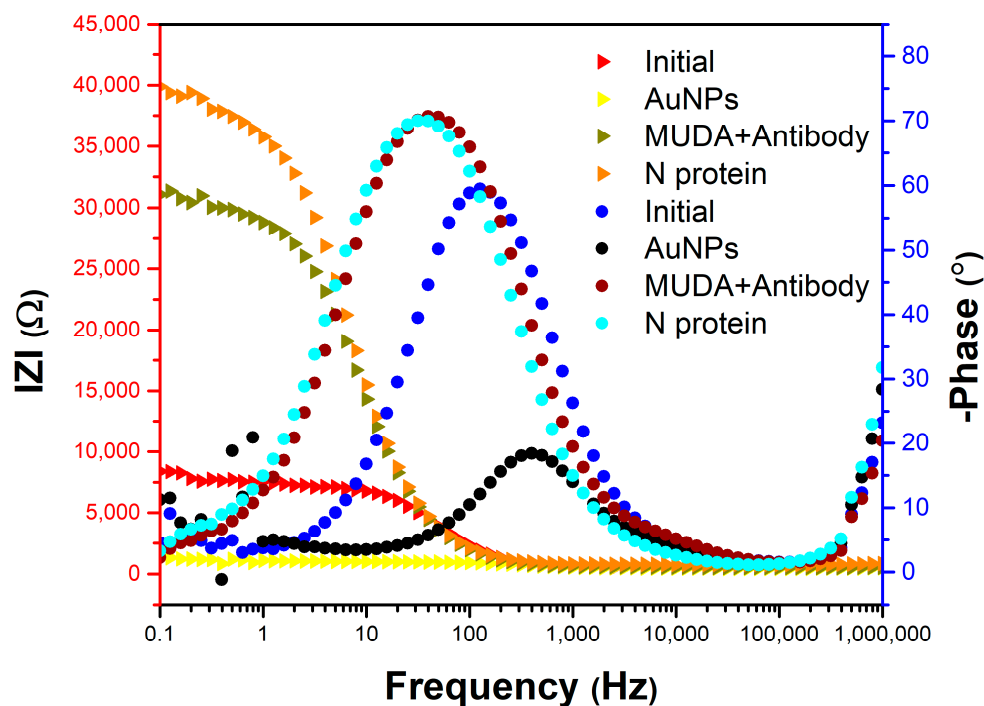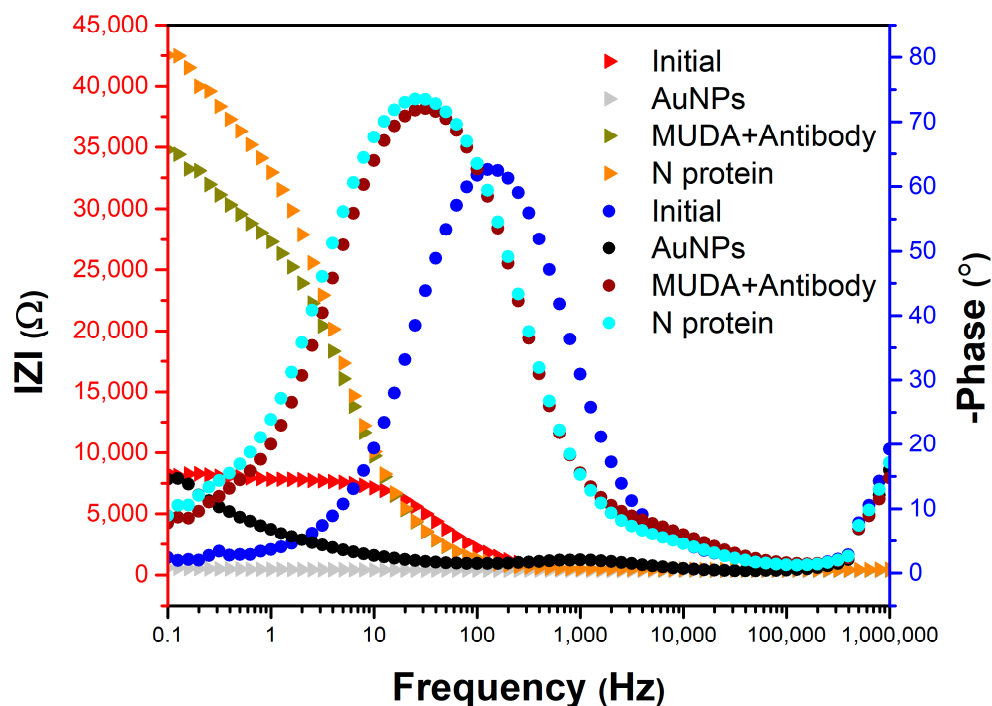
4. Discussion

We started this study focusing on the fabrication process optimization for in-house bioprinted flexible and rigid electrochemical carbon-based sensors. We customized the process in different stages of development, from design to materials and even printing.

The fabrication process for rigid sensors was simpler than the one for flexible sensors (Figure 1), as it did not require a thin sheet of Kapton® or the transfer from the rigid support substrate. The Kapton® sheet could be maintained, or the sensors could be directly printed on the rigid substrate, noting that they need to be isolating materials.

As mentioned in Section 3.1, we tested the fabrication process workflow on two designs (Figure 2a,c), each with several variations to determine the optimal configuration. We found that the optimal choice was printing the working and counter electrodes fully out of carbon paste, with electrical routes and pads, while the reference electrode should remain out of silver paste.

The next important decision was to choose the AuNP decoration method and parameters that would suit our needs. SEM characterization helped us identify two viable sensors that we used, in the end, to assess the biosensors' functionality by performing surface functionalization with specific anti-N-protein antibodies for SARS-CoV 2 virus. The size of the AuNPs did not seem to considerably affect the sensors' performance. Their density on the other hand had a greater impact on the performance, as it increased the active surface, thus increasing the conductivity, which led to greater sensor sensitivity, confirmed using the CV and the EIS measurements. A small difference in the AuNP densities of the S6/02.08 and S7/02.08 sensors could induce slight differences in the sensors' EIS behavior, as observed in Figures 6 and 7.

5. Conclusions

We successfully developed a customizable fabrication process for flexible (and rigid) 3D-printed carbon-based biosensors for electrochemical impedance spectroscopy.

The preliminary results proved to be promising, as the EIS study, the Nyquist diagram to be more precise, clearly showed the N-protein detection for both sensors at nearly the same value (-Z″ ≈ 16,750 Ω) and confirmed the sensors' functionality. The presence of the N-protein was also confirmed with Raman spectra, the C–S and S–S vibrations of Met and Cys, and the S–H vibrations of cysteine being localized around $1300\,\mathrm{cm}^{-1}$ and $1600\,\mathrm{cm}^{-1}$.

Future research will involve extending the use of these in-house 3D-printed flexible carbon-based electrochemical sensors to detect other viruses and drugs or even setting up a controlled drug release device, integrated into a smart wound dressing. As these flexible carbon-based sensors were designed for future integration in smart wound dressings, we will further work on the development of microfluidic platforms that will encapsulate the sensors. The next steps will involve running more tests on the sensors with different concentrations of the SARS-CoV-2 nucleocapsid protein solution. Additionally, we will perform more N-protein detection experiments with the successive addition of N-protein after each sensor functionalization step to test for non-specific interactions. We shall also conduct some interference studies, adding more relevant interfering agents in the human blood plasma samples to test the reliability and effect on the sensors.

Author Contributions: Conceptualization, C.M.; data curation, E.C. and A.M.; funding acquisition, M.A.; investigation, C.M., B.T., A.M., O.B., C.P. and P.P.; methodology, C.M., P.P., B.T., O.B., C.P. and M.A.; project administration, M.A.; software, C.M. and B.T.; supervision, M.A.; visualization, C.M. and O.B.; writing—original draft preparation, C.M., T.B., P.P., E.C., B.T., O.B., C.P., A.M. and M.A.; writing—review and editing, C.M., E.C. and M.A. All authors have read and agreed to the published version of the manuscript.

Institutional Review Board Statement: Not applicable.

Informed Consent Statement: Not applicable.

Data Availability Statement: The data that support the findings of this study are available from the corresponding author upon reasonable request.

Conflicts of Interest: The authors declare no conflict of interest.

Appendix A

Figure A1. Cyclic voltammogram for the S6/02.08 sensor with measurements after AuNP decoration, MUDA functionalization + antibody immobilization (one step), and N-protein binding.
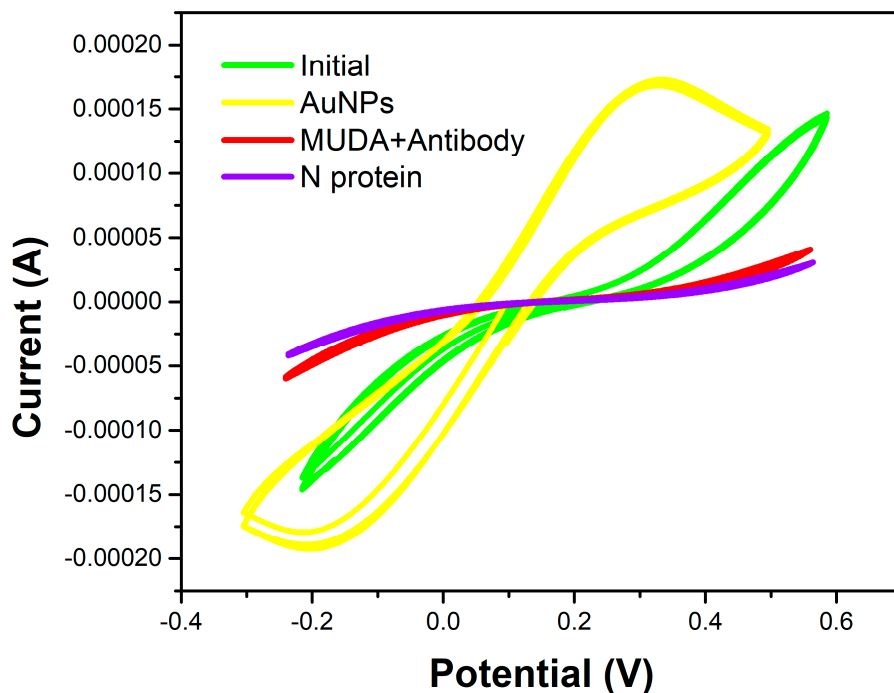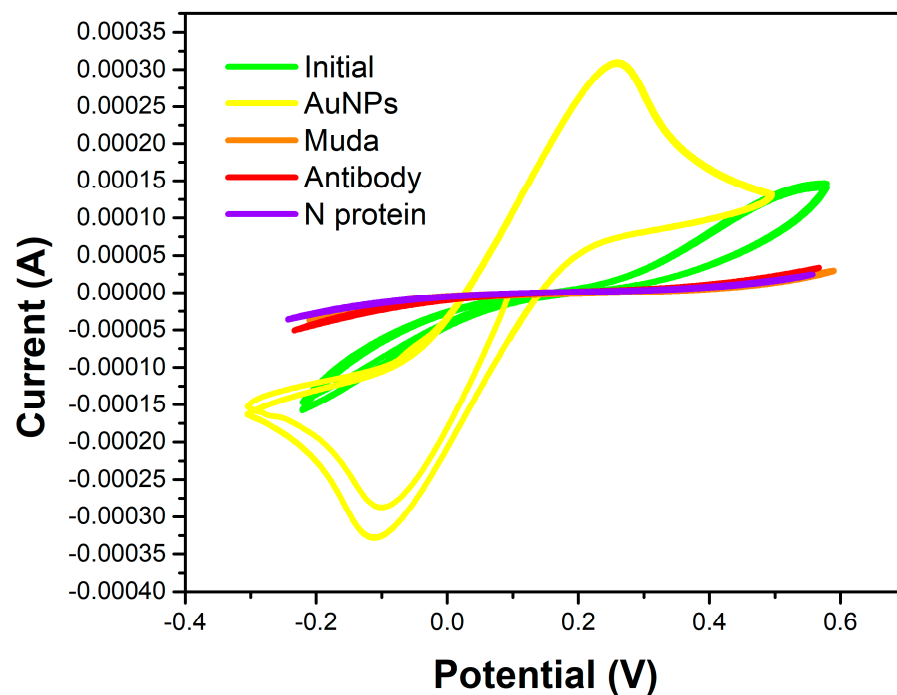

Figure A2. Cyclic voltammogram for the S7/02.08 sensor with measurements after AuNP decoration, MUDA functionalization, antibody immobilization, and N-protein binding.

References

1. Blyweert, P.; Nicolas, V.; Fierro, V.; Celzard, A. 3D Printing of Carbon-Based Materials: A Review. *Carbon* **2021**, *183*, 449–485. [CrossRef]
2. Shi, S.; Chen, Y.; Jing, J.; Yang, L. Preparation and 3D-Printing of Highly Conductive Polylactic Acid/Carbon Nanotube Nanocomposites via Local Enrichment Strategy. *RSC Adv.* **2019**, *9*, 29980–29986. [CrossRef] [PubMed]
3. Sanei, S.H.R.; Popescu, D. 3D-Printed Carbon Fiber Reinforced Polymer Composites: A Systematic Review. *J. Compos. Sci.* **2020**, *4*, 98. [CrossRef]
4. Amouzadeh Tabrizi, M.; Acedo, P. An Electrochemical Impedance Spectroscopy-Based Aptasensor for the Determination of SARS-CoV-2-RBD Using a Carbon Nanofiber–Gold Nanocomposite Modified Screen-Printed Electrode. *Biosensors* **2022**, *12*, 142. [CrossRef]
5. Callanan, C.J.; Hsu, L.; McGee, A. Formulation and Evaluation of Carbon Black 3D Printing Materials. In Proceedings of the OCEANS 2018 MTS/IEEE Charleston, Charleston, SC, USA, 22–25 October 2018; pp. 1–7. [CrossRef]
6. Fabiani, L.; Saroglia, M.; Galatà, G.; De Santis, R.; Fillo, S.; Luca, V.; Faggioni, G.; D'Amore, N.; Regalbuto, E.; Salvatori, P.; et al. Magnetic Beads Combined with Carbon Black-Based Screen-Printed Electrodes for COVID-19: A Reliable and Miniaturized Electrochemical Immunosensor for SARS-CoV-2 Detection in Saliva. *Biosens. Bioelectron.* **2021**, *171*, 112686. [CrossRef]
7. Guo, H.; Lv, R.; Bai, S. Recent advances on 3D Printing Graphene-Based Composites. *Nano Mater. Sci.* **2019**, *1*, 101–115. [CrossRef]
8. Silva, L.R.G.; Stefano, J.S.; Orzari, L.O.; Brazaca, L.C.; Carrilho, E.; Marcolino-Junior, L.H.; Bergamini, M.F.; Munoz, R.A.A.; Janegitz, B.C. Electrochemical Biosensor for SARS-CoV-2 CDNA Detection Using AuPs-Modified 3D-Printed Graphene Electrodes. *Biosensors* **2022**, *12*, 622. [CrossRef]
9. Remaggi, G.; Zaccarelli, A.; Elviri, L. 3D Printing Technologies in Biosensors Production: Recent Developments. *Chemosensors* **2022**, *10*, 65. [CrossRef]
10. Omar, M.H.; Razak, K.A.; Wahab, M.N.A.; Hamzah, H.H. Recent Progress of Conductive 3D-Printed Electrodes Based upon Polymers/Carbon Nanomaterials Using a Fused Deposition Modelling (FDM) Method as Emerging Electrochemical Sensing Devices. *RSC Adv.* **2021**, *11*, 16557–16571. [CrossRef]
11. Dăscălescu, D.; Apetrei, C. Development of a Novel Electrochemical Biosensor Based on Organized Mesoporous Carbon and Laccase for the Detection of Serotonin in Food Supplements. *Chemosensors* **2022**, *10*, 365. [CrossRef]
12. Ben Abdallah, Z.; Sghaier, H.; Gammoudi, I.; Moroté, F.; Cassagnère, S.; Romo, L.; Béven, L.; Grauby-Heywang, C.; Cohen-Bouhacina, T. Design, Elaboration, and Characterization of an Immunosensor for the Detection of a Fungal Toxin in Foodstuff Analyses. *Chemosensors* **2022**, *10*, 137. [CrossRef]
13. Talbi, M.; Al-Hamry, A.; Teixeira, P.R.; Paterno, L.G.; Ali, M.B.; Kanoun, O. Enhanced Nitrite Detection by a Carbon Screen Printed Electrode Modified with Photochemically-Made AuNPs. *Chemosensors* **2022**, *10*, 40. [CrossRef]
14. Mei, C.J.; Yusof, N.A.; Alang Ahmad, S.A. Electrochemical Determination of Lead & Copper Ions Using Thiolated Calix[4]arene-Modified Screen-Printed Carbon Electrode. *Chemosensors* **2021**, *9*, 157. [CrossRef]
15. Enache, T.A.; Enculescu, M.; Bunea, M.-C.; Zubillaga, E.A.; Tellechea, E.; Aresti, M.; Lasheras, M.; Asensio, A.C.; Diculescu, V.C. Carbon Inks-Based Screen-Printed Electrodes for Qualitative Analysis of Amino Acids. *Int. J. Mol. Sci.* **2023**, *24*, 1129. [CrossRef] [PubMed]
16. Xu, G.; Lu, Y.; Cheng, C.; Li, X.; Xu, J.; Liu, Z.; Liu, J.; Liu, G.; Shi, Z.; Chen, Z.; et al. Battery-Free and Wireless Smart Wound Dressing for Wound Infection Monitoring and Electrically Controlled On-Demand Drug Delivery. *Adv. Funct. Mater.* **2021**, *31*, 2100852. [CrossRef]
17. de Campos, A.M.; Silva, R.R.; Calegaro, M.L.; Raymundo-Pereira, P.A. Design and Fabrication of Flexible Copper Sensor Decorated with Bismuth Micro/Nanodentrites to Detect Lead and Cadmium in Noninvasive Samples of Sweat. *Chemosensors* **2022**, *10*, 446. [CrossRef]
18. Mathew, M.; Radhakrishnan, S.; Vaidyanathan, A.; Chakraborty, B.; Rout, C.S. Flexible and Wearable Electrochemical Biosensors Based on Two-Dimensional Materials: Recent Developments. *Anal. Bioanal. Chem.* **2021**, *413*, 727–762. [CrossRef]
19. Ma, J.; Zhang, C.; Hong, X.; Liu, J. Incorporating Cerium Vanadate into Multi-Walled Carbon Nanotubes for Fabrication of Sensitive Electrochemical Sensors toward Sulfamethazine Determination in Water Samples. *Chemosensors* **2023**, *11*, 64. [CrossRef]
20. Zhao, Y.; Tao, Y.; Huang, Q.; Huang, J.; Kuang, J.; Gu, R.; Zeng, P.; Li, H.-Y.; Liang, H.; Liu, H. Electrochemical Biosensor Employing Bi2S3 Nanocrystals-Modified Electrode for Bladder Cancer Biomarker Detection. *Chemosensors* **2022**, *10*, 48. [CrossRef]
21. de Sá, A.C.; Barbosa, S.C.; Raymundo-Pereira, P.A.; Wilson, D.; Shimizu, F.M.; Raposo, M.; Oliveira, O.N. Flexible Carbon Electrodes for Electrochemical Detection of Bisphenol-A, Hydroquinone and Catechol in Water Samples. *Chemosensors* **2020**, *8*, 103. [CrossRef]
22. Gao, Y.; Nguyen, D.T.; Yeo, T.; Lim, S.B.; Tan, W.X.; Madden, L.E.; Jin, L.; Long, J.Y.K.; Aloweni, F.A.B.; Liew, Y.J.A.; et al. A Flexible Multiplexed Immunosensor for Point-of-Care in Situ Wound Monitoring. *Sci. Adv.* **2021**, *7*, eabg9614. [CrossRef] [PubMed]
23. Zhao, A.; Zhang, Z.; Zhang, P.; Xiao, S.; Wang, L.; Dong, Y.; Yuan, H.; Li, P.; Sun, Y.; Jiang, X.; et al. 3D Nanoporous Gold Scaffold Supported on Graphene Paper: Freestanding and Flexible Electrode with High Loading of Ultrafine PtCo Alloy Nanoparticles for Electrochemical Glucose Sensing. *Anal. Chim. Acta* **2016**, *938*, 63–71. [CrossRef] [PubMed]
24. Lee, H.; Choi, T.K.; Lee, Y.B.; Cho, H.R.; Ghaffari, R.; Wang, L.; Choi, H.J.; Chung, T.D.; Lu, N.; Hyeon, T.; et al. A Graphene-Based Electrochemical Device with Thermoresponsive Microneedles for Diabetes Monitoring and Therapy. *Nat. Nanotechnol.* **2016**, *11*, 566–572. [CrossRef]

25. Britton, J.; Krukiewicz, K.; Chandran, M.; Fernandez, J.; Poudel, A.; Sarasua, J.-R.; FitzGerald, U.; Biggs, M.J.P. A Flexible Strain-Responsive Sensor Fabricated from a Biocompatible Electronic Ink via an Additive-Manufacturing Process. *Mater. Des.* **2021**, *206*, 109700. [CrossRef]

26. Tang, K.; Ma, H.; Tian, Y.; Liu, Z.; Jin, H.; Hou, S.; Zhou, K.; Tian, X. 3D Printed Hybrid-Dimensional Electrodes for Flexible Micro-Supercapacitors with Superior Electrochemical Behaviours. *Virtual Phys. Prototyp.* **2020**, *15*, 511–519. [CrossRef]

27. Silva-Neto, H.A.; Dias, A.A.; Coltro, W.K.T. 3D-Printed Electrochemical Platform with Multi-Purpose Carbon Black Sensing Electrodes. *Microchim. Acta* **2022**, *189*, 235. [CrossRef] [PubMed]

28. Higa, A.M.; Mambrini, G.P.; Ierich, J.C.M.; Garcia, P.S.; Scramin, J.A.; Peroni, L.A.; Okuda-Shinagawa, N.M.; Teresa Machini, M.; Trivinho-Strixino, F.; Leite, F.L. Peptide-Conjugated Silver Nanoparticle for Autoantibody Recognition. *J. Nanosci. Nanotechnol.* **2019**, *19*, 7564–7573. [CrossRef]

29. Drobysh, M.; Liustrovaite, V.; Baradoke, A.; Viter, R.; Chen, C.-F.; Ramanavicius, A.; Ramanaviciene, A. Determination of rSpike Protein by Specific Antibodies with Screen-Printed Carbon Electrode Modified by Electrodeposited Gold Nanostructures. *Biosensors* **2022**, *12*, 593. [CrossRef]

30. Ferrari, A.C. Raman spectroscopy of graphene and graphite: Disorder, Electron–Phonon Coupling, Doping and Nonadiabatic Effects. *Solid State Commun.* **2007**, *143*, 47–57. [CrossRef]

31. Thomas, G.J. Raman Spectroscopy of Protein and Nucleic Acid Assemblies. *Annu. Rev. Biophys. Biomol. Struct.* **1999**, *28*, 1–27. [CrossRef]